TECHNICAL REPORTS

nature neuroscience

NeuroGrid: recording action potentials from the surface of the brain

Dion Khodagholy[1], Jennifer N Gelinas[1], Thomas Thesen[2], Werner Doyle[2], Orrin Devinsky[2], George G Malliaras[3] & György Buzsáki[1]

Recording from neural networks at the resolution of action potentials is critical for understanding how information is processed in the brain. Here, we address this challenge by developing an organic material–based, ultraconformable, biocompatible and scalable neural interface array (the 'NeuroGrid') that can record both local field potentials (LFPs) and action potentials from superficial cortical neurons without penetrating the brain surface. Spikes with features of interneurons and pyramidal cells were simultaneously acquired by multiple neighboring electrodes of the NeuroGrid, allowing for the isolation of putative single neurons in rats. Spiking activity demonstrated consistent phase modulation by ongoing brain oscillations and was stable in recordings exceeding 1 week's duration. We also recorded LFP-modulated spiking activity intraoperatively in patients undergoing epilepsy surgery. The NeuroGrid constitutes an effective method for large-scale, stable recording of neuronal spikes in concert with local population synaptic activity, enhancing comprehension of neural processes across spatiotemporal scales and potentially facilitating diagnosis and therapy for brain disorders.

The main form of communication among neurons in the brain occurs through action potentials ('spikes'). Understanding the mechanisms that translate spikes of individual neurons into perceptions, thoughts and actions requires the ability to monitor large populations of neurons at the spatial and temporal resolution of their interactions[1–3]. Action potentials generate a transmembrane potential that can be detected by an electrical conductor, such as a wire, in the extracellular medium at close proximity to the neuron[4]. Direct electrical coupling between sensor and neural tissue allows temporally precise recording of single-unit firing in combination with population synaptic activity, often in the form of brain oscillations. Recording of multiple single extracellular action potentials ('units') is possible using wire 'tetrode' arrays[5] or silicon probes[6–8]. Although these penetrating electrodes can isolate signals from individual neurons and have yielded important insight into neural correlates of behavior, large arrays of penetrating electrodes cause damage to brain tissue and recording instability[8,9]. These features restrict recording to a small neuronal volume of interest and limit the monitoring of large-scale neural dynamics occurring over contiguous areas of cortex.

Simultaneous intra- and extracellular recordings from hippocampal neurons *in vivo* have demonstrated that action potentials of hippocampal pyramidal neurons can be detected up to 150 µm laterally from the soma but at distances exceeding 200 µm when the recording sites are parallel with the somatodendritic axis[10–12]. We therefore hypothesized that action potentials could be recorded from the surface of the cortex without penetration of the brain. Although subdural recording of LFP is well established in experimental animals and human patients[13], currently available electrode arrays do not conform to the curvilinear surface of the brain, decreasing the stability and efficiency of the electrical and mechanical contacts. Moreover, owing to electrode size and spacing relative to underlying neurons, such arrays integrate the activity of numerous neurons over a large volume of neural tissue. These factors prevent detection of units from the cortical surface[14]. To overcome these limitations, we developed a novel, organic material–based, ultraconformable, biocompatible and scalable neural interface array (the 'NeuroGrid') with neuron-sized-density electrodes. We demonstrate that the NeuroGrid can chronically record LFP and action potentials from superficial cortical neurons without penetrating the brain surface both in behaving rats and in human patients undergoing surgery to treat epilepsy.

RESULTS

We recorded action potentials from the surface of the neocortex and hippocampus with the NeuroGrid. We have determined that the ability of the array to isolate single-neuron action potentials is a product of several design elements: (i) recording electrode density that matches the average size of neuronal bodies and neuronal density (10×10-µm^2 electrode surface area and 30-µm interelectrode spacing; **Fig. 1a** inset and **Supplementary Fig. 1a**); (ii) use of poly(3,4-ethylenedioxythiophene) doped with poly(styrenesulfonate) (PEDOT:PSS) as the interface material, which substantially (by an order of magnitude) decreases electrochemical impedance mismatch between tissue and electrodes as a result of its mixed electronic and ionic conductivity and high ionic mobility[15,16] (**Supplementary Fig. 1d**); (iii) encapsulation with parylene C, to allow microfabrication of a

[1]NYU Neuroscience Institute, School of Medicine, New York University, New York, New York, USA. [2]Department of Neurology, Comprehensive Epilepsy Center, New York University, New York, New York, USA. [3]Department of Bioelectronics, Ecole Nationale Supérieure des Mines, Microelectronics Center of Provence–Saint-Etienne School of Mines (CMP-EMSE), MOC, Gardanne, France. Correspondence should be addressed to G.B. (gyorgy.buzsaki@nyumc.org).

Received 14 July; accepted 21 November; published online 22 December 2014; doi:10.1038/nn.3905

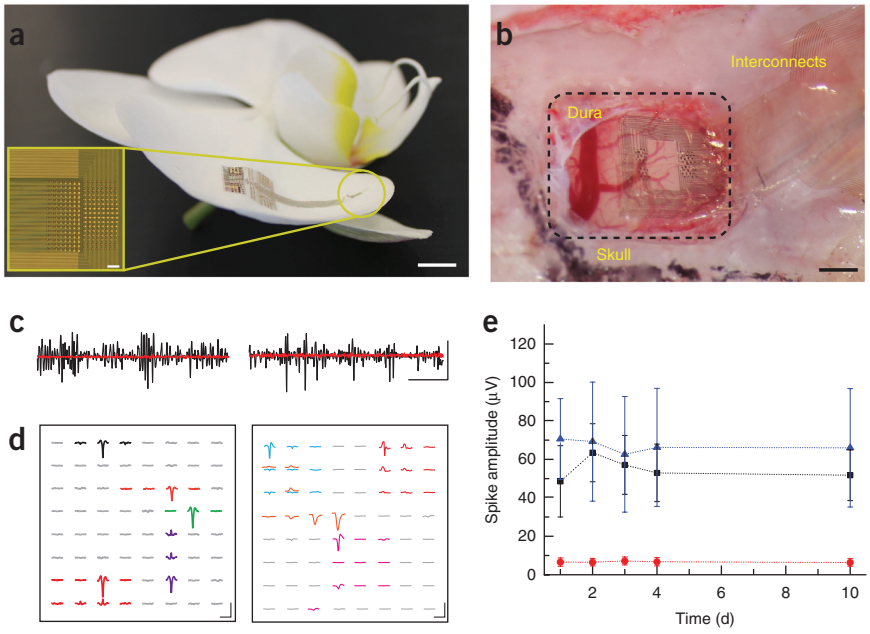

Figure 1 NeuroGrid structure and spike recordings in freely moving rats. (**a**) The NeuroGrid conforms to the surface of an orchid petal (scale bar, 5 mm). Inset, optical micrograph of a 256-electrode NeuroGrid (scale bar, 100 μm). Electrodes are 10 × 10 μm^2 with 30-μm interelectrode spacing. (**b**) The NeuroGrid conforms to the surface of the rat somatosensory cortex. The edge of the resected dura is visible at top left of the craniotomy (scale bar, 1 mm). (**c**) High-pass-filtered (f_c = 500 Hz) time traces recorded in a freely moving rat from the surface of cortex (left) and hippocampus (right) in black. Corresponding postmortem filtered traces (r.m.s. noise = 3 μV at spike bandwidth) are in red (scale bars, 10 ms × 50 μV). (**d**) Examples of the spatial extent of extracellular action potentials in cortex (left) and hippocampus (right) over the geometry of the NeuroGrid by spike-triggered averaging during the detected spike times (scale bars, 1.5 ms × 50 μV). (**e**) Mean and s.d. of the amplitude of detected action potential waveforms across 10 d of recording. The average amplitude and the variability of hippocampal waveforms (blue) are larger than those of cortical waveforms (black). The red curve demonstrates the spike detection threshold (r.m.s. noise = 8 μV at 0.1–7,500 Hz).

thin (4 μm) and ultraconformable structure that can closely adhere to complex curvilinear surfaces (**Fig. 1a** and **Supplementary Fig. 1b**). The entire microfabrication process was based on generic photolithographic patterning[17,18]. Platinum and gold, used as interconnects and pads, were embedded at the mechanical neutral plane of the device (2 μm depth) to generate a robust mechanical structure able to conform to a small bending radius (**Supplementary Fig. 1b**). These metallic structures were completely covered with PEDOT:PSS or parylene C to prevent any exposure to brain tissue. Gold was used as an inert substrate for PEDOT:PSS deposition coupled with platinum as a bonding pad, thereby eliminating the need for bulky connectors between the PEDOT:PSS-based flexible electrodes and conventional rigid electronic components. These design elements result in low noise, high stability of electrode response over time and high signal-to-noise ratio (**Supplementary Figs. 1c,d** and **2**).

In rats, the NeuroGrid was placed on the cortical surface exposed by removal of dura mater (**Fig. 1b**) or on the alvear surface of the hippocampus after removal of a small piece of neocortex. To anchor the NeuroGrid for chronic *in vivo* use after placement, it was covered with bioabsorbable gelatin compressed sponge (Gelfoam) and the craniotomy was sealed with paraffin. Physiological recordings were performed while rats engaged in normal behavior in their home cage (**Supplementary Video 1**). Signals were amplified, multiplexed and digitized using a head-stage mounted directly on the NeuroGrid to allow free movement of the animal. High-pass-filtered (500 Hz) traces from the surface of somatosensory cortex or hippocampus yielded observable spiking activity (**Fig. 1c**), except at sites above major blood vessels (**Supplementary Fig. 3a,b**) and in postmortem recordings. Spikes with amplitude at least 5 times larger than the root mean square (r.m.s.) of the background activity were selected for semiautomatic

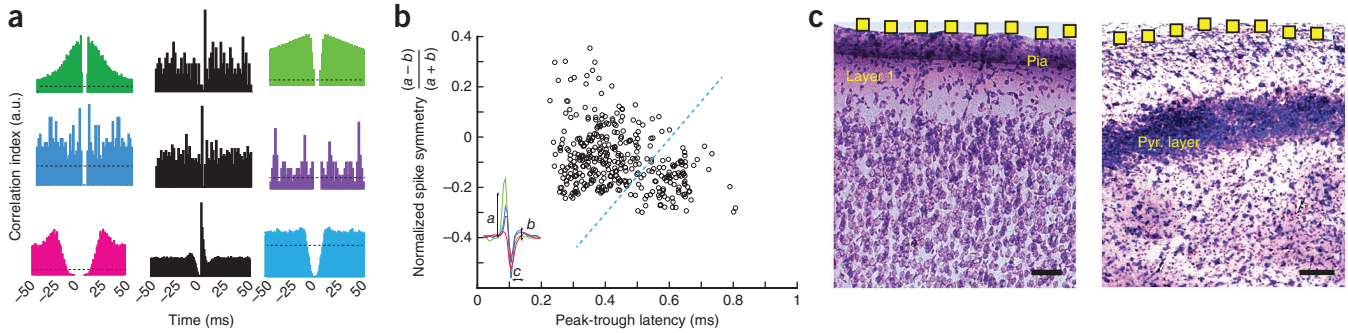

Figure 2 Neuron clustering and spike-waveform characterization. (**a**) Sample autocorrelograms (in color) of putative single-unit spiking from hippocampus (top two rows) and cortex (bottom row). Spiking cross-correlations (black) demonstrate excitatory and inhibitory interactions between putative single-unit pairs. (**b**) Scatterplot of waveform characteristics of putative single units recorded with the NeuroGrid reveals two broad clusters. Neurons were clustered according to waveform symmetry and mean wide-band spike width. Each symbol corresponds to an average spike waveform of a putative isolated neuron. The symmetry of the waveform is defined by the comparison of the peaks of the spike (*a* and *b*), and the spike duration is defined by the latency of spike peak to trough (*c*), as illustrated in the inset at bottom left. (**c**) Nissl-stained coronal sections of cortex (left) and hippocampus (right) deep to NeuroGrid placement. Electrode location on the surface is estimated in yellow (electrodes not to scale; scale bars, 100 μm; pyr., pyramidal).

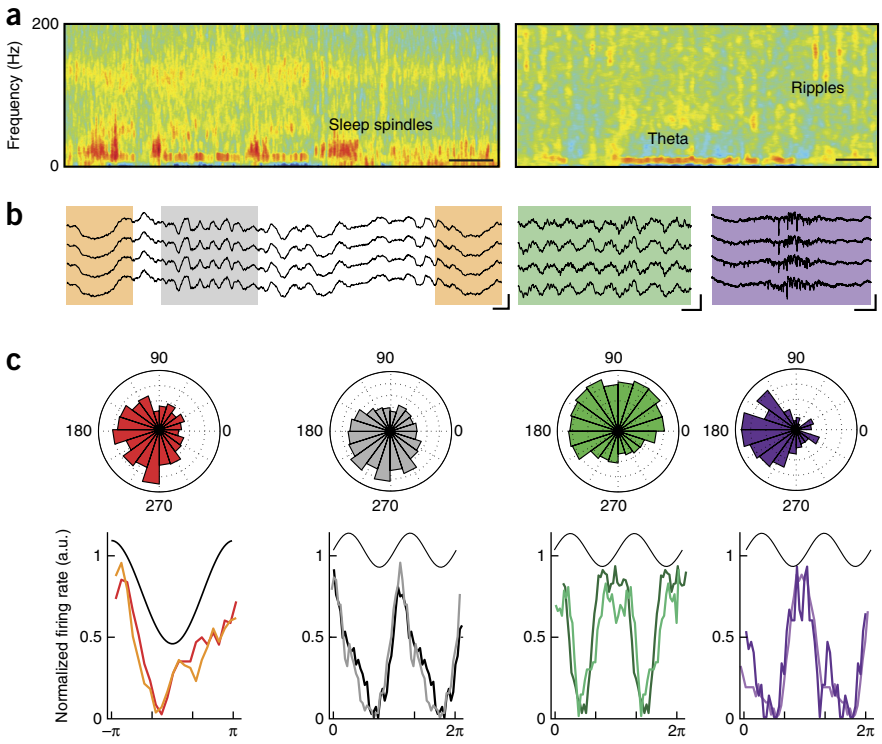

Figure 3 Phase modulation of NeuroGrid spikes by brain oscillations. (**a**) Time-frequency spectrogram of LFP recorded by the NeuroGrid during sleep in cortex (left) and hippocampus (right). The cortical spectrogram during an NREM epoch contains sleep spindles (9–16 Hz) and slow oscillations (2–4 Hz). The hippocampal spectrogram manifests theta oscillations during a REM epoch (middle of panel) and ripples (100–150 Hz) during an NREM epoch (right of panel). Scale bars, 10 s. Colors represent normalized power, with warmer colors indicating higher power. (**b**) Sample raw LFP traces demonstrating each oscillation (orange = slow oscillation, gray = spindle, scale bars, 100 ms × 250 μV; green = theta, scale bars, 250 ms × 250 μV; purple = ripple, scale bars, 100 ms × 100 μV). (**c**) Polar plots show phase-locking of sample neural firing to oscillations in cortex (left; slow oscillation and spindles) and hippocampus (right; theta and ripples). Histograms corresponding to the above polar plots for each type of cortical and hippocampal oscillation on the initial day of recording (matching color trace) and 10 d later (lighter color trace) demonstrate consistent phase modulation of units over time. Neocortical and hippocampal recordings are from different rats.

clustering and identification of putative single units[12]. Spikes were detected on multiple electrodes (corresponding to a recording area encompassing approximately 0.25–1 mm^2), with relatively higher-amplitude units in the hippocampus compared to the neocortex (**Supplementary Table 1**).

The spatial extent of the action potential waveforms from putative individual neurons was determined by spike-triggered averaging across all sites of the NeuroGrid. The waveforms typically had a localized negative peak at the detection site, with polarity reversal at adjacent sites (**Fig. 1d**). This appearance is consistent with previous modeling and experimental data on the geometry of sinks and sources in the extracellular space[10,19]. The morphology of individual waveforms was consistent across several days of recording (**Supplementary Figs. 3c** and **4b**). Average spike waveform amplitude was also maintained over 10 d of recording, with no increase in spike detection threshold (**Fig. 1e**). *In vivo* r.m.s. noise as assessed in postmortem animals was 3 μV for spike bandwidth and 8 μV at recording bandwidth (0.1–7,500 Hz). These results reflect the ability of the NeuroGrid to stably monitor the activity of individual neurons over time with minimal physiologic disruption.

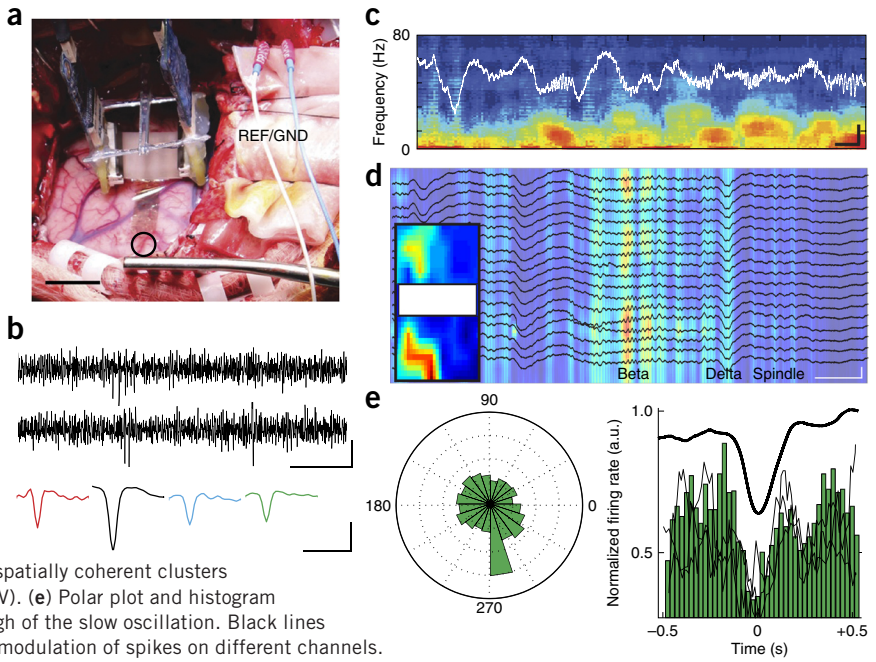

Figure 4 Intraoperative NeuroGrid recording of LFP and spikes in epilepsy patients. (**a**) Surgical placement of the NeuroGrid on the surface of human brain (open circle). Acquisition electronics are suspended above the cortical surface. Two stainless-steel needle electrodes served as reference and ground electrodes (denoted REF and GND, respectively) adjacent to the craniotomy (scale bar, 2 cm). (**b**) Above, high-pass-filtered (f_c = 250 Hz) time traces of the intraoperative NeuroGrid recordings containing spiking activity (scale bars, 20 ms × 40 μV). Below, sample spike waveforms obtained by spike-triggered averaging of spikes from different recording sites (colors; scale bars, 1 ms × 40 μV). (**c**) Sample time-frequency spectrogram of intraoperative recordings under anesthesia from an epilepsy patient (scale bars, 500 ms × 500 μV). (**d**) Sample multichannel LFP recording during intraoperative anesthesia (black traces) overlaid on time-frequency spectrogram filtered at beta frequency (18–25 Hz). Areas with high beta-frequency power are located in spatially coherent clusters on the NeuroGrid (inset; scale bars, 500 ms × 750 μV). (**e**) Polar plot and histogram demonstrating decreased spike firing during the trough of the slow oscillation. Black lines superimposed on the histogram correspond to phase modulation of spikes on different channels.

Over what spatial distance can the NeuroGrid detect neuronal spikes? To address this question, we analyzed features of spikes acquired from rat neocortex and hippocampus. Autocorrelation of spike trains is routinely used to ensure separation of spikes emanating from neighboring neurons[12]. Clustered spikes detected by the NeuroGrid generated autocorrelograms with typical neuronal refractory periods (**Fig. 2a**, in color). Isolated putative single units exhibited a range of firing rates (0.1–60 Hz), and some hippocampal units had autocorrelograms with peaks at short interspike intervals (**Fig. 2a**, in purple), characteristic of burst firing of pyramidal cells[20]. To directly validate the physiologic nature of spiking activity recorded from the surface with the NeuroGrid, we simultaneously detected some of these spikes using a silicon probe inserted into adjacent brain parenchyma (<200 μm deep from the surface; **Supplementary Fig. 5e**). Spikes recorded by the NeuroGrid exhibited a wide distribution of morphologic features (**Fig. 2b**), suggesting that the recorded units are likely to reflect activity of both layer 1 interneurons and also pyramidal cells and fast-firing interneurons in deeper layers[21,22]. Very-short-duration (<0.5 ms), 'triphasic', symmetric waveforms, consistent with axonal spikes[23], were occasionally identified, but their amplitude was typically below the unit detection threshold.

Short-timescale cross-correlations between unit pairs further supported the presence of pyramidal cells among the clustered units. A reference neuron whose spikes consistently preceded spikes from a second neuron with less than 3 ms latency was assumed to be excitatory, whereas a reference neuron whose spikes were consistently followed by transiently decreased spiking probability of a second neuron was considered inhibitory[24]. Both excitatory and inhibitory interactions were observed between cortical and hippocampal clustered units (**Fig. 2a**, in black). Although these physiological methods are indirect measures of neuronal connectivity[24], they suggest that the NeuroGrid can also record spikes of pyramidal cells from the superficial layers of the neocortex and pyramidal layer of the hippocampus, extending its spatial radius of neuron spike recording ability to 150–200 μm (**Fig. 2c**).

The NeuroGrid recorded LFP oscillatory events over a wide range of frequencies (**Fig. 3a**,**b**). As expected, during non–rapid eye movement (NREM) sleep, neocortical units robustly decreased their spiking rates at the trough of the locally recorded slow oscillations[25,26] and were also phase-locked to sleep spindles[26,27] (**Fig. 3c**, orange and gray). Most hippocampal units were phase-modulated by theta oscillations and, in their absence, by sharp wave–ripple complexes (**Fig. 3c**, green and purple)[28]. Phase-locking of units to LFP was observable over several days of recording (**Fig. 3c**, histograms).

After establishing the recording ability of the NeuroGrid in rats, we performed intraoperative recordings over mid-superior temporal gyrus in two human patients undergoing epilepsy surgery. The NeuroGrid was placed on the pial surface after removal of the chronic diagnostic subdural grid in one patient, and after intraoperative clinical electrocorticography (EcoG) and tumor resection in the other patient (**Fig. 4a**). Because of its conformability and hydrophobic surface (parylene C), the NeuroGrid made stable electrical and mechanical contact with the cortical surface despite brain pulsations. Cortical slow oscillations interspersed with higher-frequency activity were observed, commensurate with surgical anesthesia. Beta-frequency oscillations exhibited differential power across channels and formed spatially coherent clusters of activity (**Fig. 4**). High-pass-filtered traces revealed spiking activity (**Fig. 4b**). Although the limited intraoperative recording time (8 and 20 min) and the lower amplitude of the spikes in human as compared to rodent recordings precluded reliable clustering of putative single neurons, spikes displayed typical waveform patterns (**Fig. 4b**) and were reliably phase-modulated by cortical slow oscillations (**Fig. 4e**), confirming the physiologic nature of the activity.

DISCUSSION

Our findings demonstrate that it is possible to record action potentials from superficial cortical layers of rodents and humans with high fidelity and extended duration using a nonpenetrating surface array. Although subdural ECoG electrode arrays in human subjects offer better spatiotemporal resolution than noninvasive technologies[13,14,29,30], they cannot provide data at the resolution of neural firing. Penetrating devices (such as the Utah array) enhance resolution to the level of spiking, but are limited in spatial scale and may cause permanent local tissue damage when used for long-term chronic recordings[31]. The NeuroGrid has several innovative characteristics that overcome limitations in current methods of surface recording: (i) lightweight and conformable architecture to establish stable electrical and mechanical contacts, thereby ensuring minimal damage to underlying tissue; (ii) an efficient abiotic/biotic interface resulting in a high signal-to-noise ratio and the ability to resolve spikes; and (iii) scalable, neuron-sized-density electrodes to allow isolation and characterization of multiple individual neurons' action potential waveforms across the cortical surface.

The NeuroGrid's ultrathin (4 μm) and conformable architecture allows it to closely follow the fine irregularities of the neocortical surface topography. In contrast to conventional clinical subdural ECoG arrays and flexible polyimide-based LFP probes[14,32,33], NeuroGrids can be folded and inserted into brain regions currently inaccessible to recording with surface electrodes. Clinically, this feature will facilitate acquiring data directly from the cortex lining fissures and sulci in the human brain, areas that can harbor difficult-to-diagnose epileptic lesions[34].

Because the NeuroGrid is composed of 'soft' organic electronics[16,35], it has high mechanical compatibility with brain tissue as compared to 'hard' electronics, potentially minimizing long-term impact on the cortical surface. As with all subdural recording methods, placement of the NeuroGrid requires removal of the dura mater, disrupting the normal cortical environment. However, multiple perforations can be incorporated into the NeuroGrid structure to allow free flow of cerebrospinal fluid and minimize this disruption during chronic recording. As a result of these features, we observed durable recordings from multiple single neurons for up to 10 d in rats, the typical duration of diagnostic recordings in epilepsy patients. The NeuroGrid may be capable of recording neuronal spikes over longer periods of time, as termination of recording in our subjects was not due to device failure.

Metallic electrodes conduct only electronic current, but electrophysiological signals in the brain are primarily based on ionic flux. The NeuroGrid is composed of a conducting polymer (PEDOT:PSS) that is able to conduct both ionic and electronic current, enhancing the efficiency of signal transduction[35,36]. This capacity for mixed conduction coupled with the large effective interfacing surface area of the polymer decreases the electrochemical impedance mismatch of the electrodes with brain tissue[17,37]. Hence, we were able to achieve a high signal-to-noise ratio capable of spike detection, providing substantially higher spatiotemporal resolution than was previously possible.

The NeuroGrid's neuron-sized-density recording sites enable microscopic sampling of LFP and spiking activity, thereby resolving the surface projection of individual neurons' action potentials. This data approaches the spatial resolution of voltage-sensitive dye imaging[38] but without toxic side effects, and it allows for extended measurements even from nonplanar, optically inaccessible areas. Furthermore, the NeuroGrid's micron-scale electrode spacing permits acquisition of a neuron's action potential waveform on multiple

neighboring sites and consequent source localization. This methodology has been previously successful in *in vitro* preparations using high-density planar multielectrode arrays[39–41].

Our recordings from neocortex and hippocampus demonstrate that spikes of inhibitory and excitatory neurons can be resolved, implying that the electrodes can detect neurons at least as far as 200 µm below the cortical surface. Identification of the recorded neuron types will require further experiments, including optogenetic tagging and improvements in two-dimensional neural clustering techniques. Improvement of spike clustering methods may also resolve small-amplitude axonal spikes[23], providing an opportunity to study the relationship between the activity of layer 1 afferents and spike outputs from layer 1 and layer 2 neurons. The combination of the NeuroGrid with penetrating electrodes will also allow simultaneous monitoring of interactions between neurons in superficial and deep cortical layers[42]. For instance, the NeuroGrid has the potential to record from a large fraction, or all, of the underlying layer 1 neurons, which are currently difficult to monitor at single-spike resolution by other methods.

Studies using subdural ECoG arrays provide ample evidence that the high-frequency content of the LFP is information rich[29,43,44]. Extensive studies of spectral power above 100 Hz have demonstrated, for instance, that letters of the alphabet or phonetic features of speech can be reliably decoded from the high-frequency content of cortical surface recordings[29,45]. It has been hypothesized that the high-frequency portion of the power spectrum reflects spiking activity of neuron aggregates in the underlying cortex[46]. This assertion has been difficult to verify across various neural networks because conventional surface electrodes cannot resolve spikes of single neurons. The spike-resolution data generated by the NeuroGrid can facilitate characterization of the relationship between spiking activity and the high-frequency LFP signals acquired by conventional electrodes.

The NeuroGrid structure is easily scalable to cover large surfaces: for instance, nearly the entire dorsal cortical surface in small animals, or multiple cortical areas of the human brain. Signal acquisition of such large-scale data is currently limited by lack of high-channel-count electrophysiological interfacing electronics. However, in concert with advances in high-speed electronics and data processing capacity, the amount of LFP and spike samples recorded by the NeuroGrid could be substantially increased in the future.

In summary, we have recorded action potentials from superficial cortical layers of rodents and humans with high fidelity and extended duration with highly conformable, nonpenetrating NeuroGrids. The high signal-to-noise ratio of the acquired signals permitted analysis of entrainment of spiking activity to brain oscillations. We were also able to acquire multiunit spike-resolution data from epilepsy surgery patients with this biocompatible array, highlighting its translational potential. Although numerous hurdles must be overcome for safe and reliable recording in patients to become possible[47], large-scale, chronically recorded data generated by the NeuroGrid has broad applicability to the understanding of physiologic and pathologic network activity, control of brain-machine interfaces, and therapeutic closed-loop stimulation in brain disease.

METHODS

Methods and any associated references are available in the online version of the paper.

Note: Any Supplementary Information and Source Data files are available in the online version of the paper.

ACKNOWLEDGMENTS

This work was supported by US National Institutes of Health Grants (NS074015, MH54671, MH102840), the National Science Foundation, the Mathers Foundation and the James S. McDonnell Foundation. The device fabrication was performed at Microelectronic Centre of Provence and the Cornell NanoScale Facility (CNF), a member of the National Nanotechnology Infrastructure Network, which is supported by the National Science Foundation (Grant ECCS-0335765). D.K. is supported through the Simons Foundation (junior fellow). J.G. is supported by the Pediatric Scientist Development Program through a grant from the March of Dimes Foundation. We thank M. Sessolo (University of Valencia), J. Rivnay and M. Ferro (Ecole des Mines), and A. Peyrache and G. Girardeau (NYU Langone Medical Center) for fruitful discussion. We thank M. Skvarla, R. Ilic and M. Metzler from the CNF for their technical support during device fabrication. We thank H. McKellar and A. Boomhaur for managing the institutional review board (IRB) protocol of intraoperative epilepsy patient recordings.

AUTHOR CONTRIBUTIONS

D.K., G.G.M. and G.B. conceived the project. D.K. designed, fabricated and characterized the devices. D.K. and J.N.G. did the rodent *in vivo* experiments. D.K. and J.N.G. analyzed neural data. D.K., J.N.G. and T.T. did the intraoperative patient recordings. W.D. was the attending neurosurgeon and supervised the intra-operative recordings. T.T. and O.D. supervised the epilepsy patient recordings and IRB approval process. D.K., J.N.G. and G.B. wrote the paper with input from the other authors.

COMPETING FINANCIAL INTERESTS

The authors declare no competing financial interests.

1. Buzsáki, G. Large-scale recording of neuronal ensembles. *Nat. Neurosci.* **7**, 446–451 (2004).
2. Alivisatos, A.P. *et al.* The brain activity map. *Science* **339**, 1284–1285 (2013).
3. Carandini, M. From circuits to behavior: a bridge too far? *Nat. Neurosci.* **15**, 507–509 (2012).
4. Adrian, E.D. & Moruzzi, G. Impulses in the pyramidal tract. *J. Physiol. (Lond.)* **97**, 153–199 (1939).
5. Wilson, M.A. & McNaughton, B.L. Dynamics of the hippocampal ensemble code for space. *Science* **261**, 1055–1058 (1993).
6. Wise, K.D. & Najafi, K. Microfabrication techniques for integrated sensors and microsystems. *Science* **254**, 1335–1342 (1991).
7. Buzsáki, G. & Draguhn, A. Neuronal oscillations in cortical networks. *Science* **304**, 1926–1929 (2004).
8. Campbell, P.K., Jones, K.E., Huber, R.J., Horch, K.W. & Normann, R.a. A silicon-based, three-dimensional neural interface: manufacturing processes for an intracortical electrode array. *IEEE Trans. Biomed. Eng.* **38**, 758–768 (1991).
9. Polikov, V.S., Tresco, P.A. & Reichert, W.M. Response of brain tissue to chronically implanted neural electrodes. *J. Neurosci. Methods* **148**, 1–18 (2005).
10. Gold, C., Henze, D.A., Koch, C. & Buzsáki, G. On the origin of the extracellular action potential waveform: a modeling study. *J. Neurophysiol.* **95**, 3113–3128 (2006).
11. Buzsáki, G. Somadendritic backpropagation of action potentials in cortical pyramidal cells of the awake rat. *J. Neurophysiol.* **79**, 1587–1591 (1998).
12. Harris, K.D. *et al.* Accuracy of tetrode spike separation as determined by simultaneous intracellular and extracellular measurements. *J. Neurophysiol.* **84**, 401–414 (2000).
13. Engel, A.K., Fries, P. & Singer, W. Dynamic predictions: oscillations and synchrony in top-down processing. *Nat. Rev. Neurosci.* **2**, 704–716 (2001).
14. Viventi, J. *et al.* Flexible, foldable, actively multiplexed, high-density electrode array for mapping brain activity *in vivo*. *Nat. Neurosci.* **14**, 1599–1605 (2011).
15. Stavrinidou, E. *et al.* Direct measurement of ion mobility in a conducting polymer. *Adv. Mater.* **25**, 4488–4493 (2013).
16. Owens, R.M. & Malliaras, G.G. Organic electronics at the interface with biology. *MRS Bull.* **35**, 449–456 (2010).
17. Khodagholy, D. *et al.* Highly conformable conducting polymer electrodes for *in vivo* recordings. *Adv. Mater.* **23**, 1–5 doi:10.1002/adma.201102378 (2011).
18. Khodagholy, D. *et al. In vivo* recordings of brain activity using organic transistors. *Nat. Commun.* **4**, 1575 (2013).
19. Einevoll, G.T. *et al.* Laminar population analysis: estimating firing rates and evoked synaptic activity from multielectrode recordings in rat barrel cortex. *J. Neurophysiol.* **97**, 2174–2190 (2007).
20. Ranck, J.B. Studies on single neurons and septum in dorsal hippocampal in unrestrained rats. *Exp. Neurol.* **41**, 461–531 (1973).
21. Stark, E. *et al.* Inhibition-induced theta resonance in cortical circuits. *Neuron* **80**, 1263–1276 (2013).
22. Sirota, A. *et al.* Entrainment of neocortical neurons and gamma oscillations by the hippocampal theta rhythm. *Neuron* **60**, 683–697 (2008).

23. Robbins, A.A., Fox, S.E., Holmes, G.L., Scott, R.C. & Barry, J.M. Short duration waveforms recorded extracellularly from freely moving rats are representative of axonal activity. *Front. Neural Circuits* **7**, 181 (2013).
24. Barthó, P. *et al.* Characterization of neocortical principal cells and interneurons by network interactions and extracellular features. *J. Neurophysiol.* **92**, 600–608 (2004).
25. Steriade, M., McCormick, D.A. & Sejnowski, T.J. Thalamocortical oscillations in the sleeping and aroused brain. *Science* **262**, 679–685 (1993).
26. Nir, Y. *et al.* Regional slow waves and spindles in human sleep. *Neuron* **70**, 153–169 (2011).
27. Contreras, D. *et al.* Intracellular and computational characterization of the intracortical inhibitory control of synchronized thalamic inputs *in vivo*. *J. Neurophysiol.* **78**, 335–350 (1997).
28. Csicsvari, J., Hirase, H., Czurkó, A., Mamiya, A. & Buzsáki, G. Fast network oscillations in the hippocampal CA1 region of the behaving rat. *J. Neurosci.* **19**, RC20 (1999).
29. Mesgarani, N., Cheung, C., Johnson, K. & Chang, E.F. Phonetic feature encoding in human superior temporal gyrus. *Science* **343**, 1006–1010 (2014).
30. Crone, N.E., Sinai, A. & Korzeniewska, A. High-frequency gamma oscillations and human brain mapping with electrocorticography. *Prog. Brain Res.* **159**, 275–295 (2006).
31. Waziri, A., Schevon, C. & Cappell, J. Initial surgical experience with a dense cortical microarray in epileptic patients undergoing craniotomy for subdural electrode implantation. *Neurosurgery* **64**, 540–545 (2009).
32. Rubehn, B., Bosman, C., Oostenveld, R., Fries, P. & Stieglitz, T. A MEMS-based flexible multichannel ECoG-electrode array. *J. Neural Eng.* **6**, 036003 (2009).
33. Kim, D.-H. *et al.* Dissolvable films of silk fibroin for ultrathin conformal bio-integrated electronics. *Nat. Mater.* **9**, 511–517 (2010).
34. Besson, P., Andermann, F., Dubeau, F. & Bernasconi, A. Small focal cortical dysplasia lesions are located at the bottom of a deep sulcus. *Brain* **131**, 3246–3255 (2008).
35. Berggren, M. & Richter-Dahlfors, A. Organic bioelectronics. *Adv. Mater.* **19**, 3201–3213 (2007).
36. Rivnay, J., Owens, R.M. & Malliaras, G.G. The rise of organic bioelectronics. *Chem. Mater.* **26**, 679–685 (2014).
37. Abidian, M.R. & Martin, D.C. Experimental and theoretical characterization of implantable neural microelectrodes modified with conducting polymer nanotubes. *Biomaterials* **29**, 1273–1283 (2008).
38. Peterka, D.S., Takahashi, H. & Yuste, R. Imaging voltage in neurons. *Neuron* **69**, 9–21 (2011).
39. Chichilnisky, E.J. & Baylor, D.a. Receptive-field microstructure of blue-yellow ganglion cells in primate retina. *Nat. Neurosci.* **2**, 889–893 (1999).
40. Meister, M., Pine, J. & Baylor, D.a. Multi-neuronal signals from the retina: acquisition and analysis. *J. Neurosci. Methods* **51**, 95–106 (1994).
41. Marre, O. *et al.* Mapping a complete neural population in the retina. *J. Neurosci.* **32**, 14859–14873 (2012).
42. Lee, S., Kruglikov, I., Huang, Z.J., Fishell, G. & Rudy, B. A disinhibitory circuit mediates motor integration in the somatosensory cortex. *Nat. Neurosci.* **16**, 1662–1670 (2013).
43. Thesen, T. *et al.* Sequential then interactive processing of letters and words in the left fusiform gyrus. *Nat. Commun.* **3**, 1284 (2012).
44. Bragin, A., Engel, J., Wilson, C.L., Fried, I. & Mathern, G.W. Hippocampal and entorhinal cortex high-frequency oscillations (100–500 Hz) in human epileptic brain and in kainic acid–treated rats with chronic seizures. *Epilepsia* **40**, 127–137 (1999).
45. Jacobs, J. & Kahana, M.J. Neural representations of individual stimuli in humans revealed by gamma-band electrocorticographic activity. *J. Neurosci.* **29**, 10203–10214 (2009).
46. Ray, S. & Maunsell, J.H.R. Different origins of gamma rhythm and high-gamma activity in macaque visual cortex. *PLoS Biol.* **9**, e1000610 (2011).
47. Hatsopoulos, N.G. & Donoghue, J. The science of neural interface systems. *Annu. Rev. Neurosci.* **32**, 249–266 (2009).

ONLINE METHODS

Probe fabrication and characterization. The fabrication and patterning of PEDOT:PSS-based electrodes were discussed in previous publications[17,18], resulting in devices capable of conformability around a 100-µm diameter cylinder (**Supplementary Fig. 1b**). Here we used an adapted fabrication process consisting of deposition and patterning of parylene C, Au, Pt and PEDOT:PSS films using projection exposure systems as follows: parylene C was deposited using an SCS Labcoater 2 to a thickness of 2 µm (to ensure pinhole-free films). 3-(trimethoxysilyl)propyl methacrylate (A-174 Silane) and a dilute solution of industrial cleaner (Micro-90) were used as an adhesion promoter and antiadhesion agent, respectively. The film was patterned with a 4.5-µm-thick layer of SPR220-45 (Electronic Materials) photoresist and dry etched by a plasma reactive-ion etching process (180 W, 50 sccm O_2, 3 sccm SF_6, 2 sccm CF_4 for 15 min) using an Oxford 80 plus followed by a lift-off process to pattern metal pads and interconnects. A negative photoresist, AZ nLOF 2020, was spin-coated on the parylene film at 5,500 r.p.m., baked at 115 °C for 60 s, exposed using a stepper (GCA Autostep 200 DSW i-line Wafer Stepper) and then developed using MF726 developer. Metallic layers (10 nm Ti, 150 nm Pt and 50 nm Au) were deposited using an e-beam metal evaporator (CVC SC4500) at 2.10^{-6} bars. Lift-off was performed using 1165 stripper (2 h).

To enhance the conductivity of PEDOT:PSS, a mixture of PEDOT:PSS aqueous dispersion (PH-1000 from H.C. Stark) and ethylene glycol (20:5 ml ratio) was prepared and mixed with dodecyl benzene sulfonic acid (100 µl per 50 ml) and 3-glycidoxypropyltrimethoxysilane (1 wt%) to adjust surface energy and cross-link, respectively. The resulting dispersion was spin-coated at 650 r.p.m. The films were subsequently baked at 140 °C for 1 h and then immersed in deionized water overnight to remove any excess low–molecular weight compounds. The electrodes were characterized *in vitro* using phosphate buffer solution (PBS). A tungsten wire was immersed in the electrolyte and used as the reference electrode.

Animal surgical procedure. All the animal experiments were approved by the Institutional Animal Care and Use Committee. Thirteen NeuroGrids were used in cortex ($n = 10$) and hippocampal ($n = 3$) implantations in male Long Evans rats (250–350 g; 8–11 weeks of age). Rats were housed in a regular 12 h/12 h light/dark cycle throughout the course of experimentation. Rats were housed in pairs prior to surgical procedure but separated after intracranial implantation was performed. Rats used in these experiments had no previous history of experimentation of any kind. The animals were initially anesthetized with 2% isoflurane and maintained under anesthesia with 0.75–1% isoflurane during the surgery. A series of H32 Neuronexus probes including 32 site single and quad shank probes were used to validate the surface recordings. Two tungsten wires with 100 µm diameter and 2 mm length were implanted in cerebellum to serve as ground and reference electrodes. A 2×3 mm^2 craniotomy was performed on the right hemisphere (AP = 3.5 mm, ML = 3 mm); the NeuroGrid was placed on the exposed cortical surface. A silicon probe (Neuronexus H32 series) mounted on a microdrive (277 µm per revolution) was inserted in the brain at the vicinity of the NeuroGrid. The craniotomy was covered by Gelfoam and sealed using a 10:1 mixture of paraffin and mineral oil.

Intraoperative patient recordings. Intraoperative recordings from patients undergoing epilepsy surgery recordings were approved by the Institutional Review Board at New York University Langone Medical Center (NYULMC). Patients undergoing epilepsy surgery for placement of clinical subdural ECoG arrays or resection of epileptic tissue were eligible for the study. Patients with diffuse cortical lesions or developmental disability, or who were less than 18 years of age, were excluded. In this study, patient 1 was a 24-year-old woman with nonlesional refractory epilepsy. Patient 2 was a 35-year-old woman with epilepsy related to a meningeal tumor. Informed written consent was obtained from all patients for all aspects of the protocol, including publication of photos. All electronic equipment used in the operating room was checked and approved by the Clinical Engineering Department at NYULMC. NeuroGrids, head-stages and associated cables underwent gas sterilization (97–100% ethylene oxide at 50–60 °C for 4 h followed by 12 h of detoxification) as per NYULMC protocol. Recordings lasted for a maximum of 30 min, and were performed under anesthesia as administered by the attending anesthesiologist (patient 1: dexmedetomidine, propofol, remifantyl; patient 2: sevoflurane, remifentanyl). Placement of the NeuroGrid was guided by the location of the craniotomy required for clinical diagnostic and therapeutic procedures, and on the advice of the attending neurosurgeon. Stainless steel reference and ground needle electrodes were placed in the subcutaneous tissue of the scalp adjacent to the recording area.

Data acquisition and processing. During the recording sessions in 13 rats and 2 epilepsy patients, neurophysiological signals were amplified, digitized continuously at 20 kHz using a head-stage directly attached to the probe (RHD2000 Intan technology) and stored for off-line analysis with 16-bit format. Rat LFP and unit activity were recorded in the home cage during normal behavior and sleep. The data were analyzed using MATLAB (MathWorks). An amplitude-threshold method was used to detect spikes from band-passed filtered data (0.25–2.5 kHz) and spike waveforms were retrieved from wide-band files. Cell clustering was done by an unsupervised EM algorithm (Klustakwik). Spike-LFP phase synchrony was done by a power-threshold method at the target frequency band (FMA-toolbox) according to physiological characteristics of the LFP. The instantaneous phase of the LFP was extracted by Hilbert transform and validated with wavelet (Gabor) to ensure uniform phase distribution.

Histology. Rats were killed with sodium pentobarbital and perfused via the heart with 0.9% saline followed by 10% formalin. Whole brains were extracted and sectioned using a vibratome (Leica) to create 100 µm coronal slices. Slices were mounted on gelatin-coated glass slides, stained using a Nissl staining protocol and coverslipped. A light transmission microscope (Zeiss) was used to visualize and photograph the slices. Electrode and/or probe location was reconstructed from adjacent slices.

doi:10.1038/nn.3905